

Article

Open Access



# C<sub>60</sub> and ZIF-67 synergistically modified gelatin-based nanofibrous separators for Li-S batteries

Xin Liang<sup>1,\*</sup>, Dongqing Zhao<sup>1</sup>, Lulu Wang<sup>2</sup>, Qianqian Huang<sup>1</sup>, Chonghai Deng<sup>1</sup>, Lili Wang<sup>1</sup>, Lei Hu<sup>1</sup>, Sheng Liang<sup>1</sup>, Huaxia Deng<sup>3,\*</sup>, Hongfa Xiang<sup>2,\*</sup>

<sup>1</sup>School of Energy Materials and Chemical Engineering, Hefei University, Hefei 230601, Anhui, China.

<sup>2</sup>School of Materials Science and Engineering, Engineering Research Center of High-Performance Copper Alloy Materials and Processing, Ministry of Education, Hefei University of Technology, Hefei 230009, Anhui, China.

<sup>3</sup>Department of Modern Mechanics, University of Science and Technology of China, Hefei 230026, Anhui, China.

\***Correspondence to:** Prof. Xin Liang, School of Energy Materials and Chemical Engineering, Hefei University, No.99 Jinxiu Avenue, Hefei, Anhui, China. E-mail: x.liang@hfuu.edu.cn; Prof. Huaxia Deng, Department of Modern Mechanics, University of Science and Technology of China, No.443 Huangshan Road, Hefei, Anhui, China. E-mail: hxdeng@ustc.edu.cn; Prof. Hongfa Xiang, School of Materials Science and Engineering, Hefei University of Technology, No.193 Tunxi Road, Hefei, Anhui, China. E-mail: hfxiang@hfut.edu.cn.

**How to cite this article:** Liang X, Zhao D, Wang L, Huang Q, Deng C, Wang L, Hu L, Liang S, Deng H, Xiang H. C<sub>60</sub> and ZIF-67 synergistically modified gelatin-based nanofibrous separators for Li-S batteries. *Energy Mater* 2023;3:300006. <https://dx.doi.org/10.20517/energymater.2022.63>

**Received:** 19 Oct 2022 **First Decision:** 30 Nov 2022 **Revised:** 20 Dec 2022 **Accepted:** 9 Jan 2023 **Published:** 10 Feb 2023

**Academic Editor:** Yuping Wu **Copy Editor:** Ke-Cui Yang **Production Editor:** Ke-Cui Yang

## Abstract

The lithium-sulfur (Li-S) battery has been attracting much more attention in recent years due to its high theoretical capacity and low cost, although various issues, such as the "shuttle effect" and the low use ratio of active materials, have been hindering the development and application of Li-S batteries. The separator is an important part of Li-S batteries, and its modification is a simple and effective strategy to improve the electrochemical performance of Li-S batteries. In this work, we explore separators with different functions on their two sides that have been produced by a step-by-step electrospinning method. The multifunctional separator on one side is pure gelatin, and the other side is zeolitic imidazolate framework-67 (ZIF-67)-C<sub>60</sub>-gelatin. The ZIF-67-C<sub>60</sub>-gelatin layer on the cathode side is of great importance. The chemisorption sites on it are provided by ZIF-67, and the transformation sites of lithium polysulfide are provided by C<sub>60</sub>. Gelatin, which is on the anode side, as an admirable separator material, makes the lithium flux uniform and thus prevents the generation of lithium dendrites. This type of multifunctional nanofiber separator based on double gelatin layers plays an important role in the adsorption and conversion of polysulfides, and it improves the overall performance of the Li-S battery. As a result, the Li-S batteries assembled with the prepared separator can still maintain the capacity of 888 mAh g<sup>-1</sup> after 100 cycles at 0.2 C, and the capacity



© The Author(s) 2023. **Open Access** This article is licensed under a Creative Commons Attribution 4.0 International License (<https://creativecommons.org/licenses/by/4.0/>), which permits unrestricted use, sharing, adaptation, distribution and reproduction in any medium or format, for any purpose, even commercially, as long as you give appropriate credit to the original author(s) and the source, provide a link to the Creative Commons license, and indicate if changes were made.



retention rate of the Li-S batteries is 72.9% after 400 cycles at 2 C. This simple preparation method and high-performance bilayer membrane structure provide a new route for commercial application.

**Keywords:** Gelatin-based, electrostatic spinning, modified separator, Li-S battery

## INTRODUCTION

Li-S batteries have attracted much more attention recently because of their high theoretical capacity (1675 mAh g<sup>-1</sup>) and high energy density (2600 Wh kg<sup>-1</sup>)<sup>[1]</sup>, although several problems for Li-S batteries still must be solved: (1) insulation and volume change of the charging and discharging products of the Li-S battery<sup>[2]</sup>; (2) the “shuttle effect” during charging and discharging processes<sup>[3]</sup>; and (3) lithium dendrites on the lithium anode surface<sup>[4]</sup>. Among these problems, the “shuttle effect” is the reason for the serious capacity decay of Li-S batteries<sup>[5]</sup>.

Many efforts have been made to solve the problems of Li-S batteries. From the aspect of the sulfur cathode, a common approach is designing a catalytic carbon material to load sulfur so that it encapsulates and traps lithium polysulfide before it dissolves in the electrolyte<sup>[6,7]</sup>. However, the structural design of cathode materials is complicated, the cost is high, the yield is low, and this method is difficult to apply on a large scale<sup>[8,9]</sup>. From the aspect of the lithium anode, the design of multifunctional electrolyte additives can effectively prevent the longitudinal growth of lithium dendrites<sup>[10]</sup>. Nonetheless, the amount of additive is necessarily limited. It will be consumed in repeated charge-discharge cycles and cannot guarantee long-term effective protection of the lithium anode<sup>[11,12]</sup>. From the aspect of solid electrolytes, the shuttling of lithium polysulfides can be completely suppressed by some solid electrolytes, etc., but their large interfacial resistance limits the development of batteries<sup>[13]</sup>. The separator plays the role of isolating the positive and negative electrodes while acting as the channel of lithium-ion transmission<sup>[14]</sup>. Modification of the separator is a simple and effective method to inhibit the “shuttle effect”. Therefore, more and more researchers have paid much more attention to modifying the separator in Li-S batteries to inhibit lithium polysulfide shuttling to the negative electrode<sup>[15]</sup>. HY Xiang *et al.* prepared a nanofiber membrane 3, 4-ethylene dioxyethiophene/ F co-doped poly-m-phenyleneisophthalamide (EDOT-5/F-PMIA) by electrospinning technology<sup>[16]</sup>. The pore size of the nanofiber membrane was reduced after the addition of a fluorine-containing emulsion and the EDOT. The elements S and O in the EDOT can bind to lithium polysulfide, inhibiting the “shuttle effect” of lithium polysulfide through physical constraints and chemical binding. As a result, Li-S batteries assembled with EDOT/F-PMIA separators exhibited excellent electrochemical properties. It is not enough, however, to adsorb lithium polysulfides on the surface of the separator only through physical/chemical interactions, so it is necessary to convert long-chain lithium polysulfides to prevent the accumulation of lithium polysulfides on the separator. C. Zhou *et al.* prepared a double-layer metal-organic framework - polyacrylonitrile (MOF-PAN)/rGO-PAN multifunctional nanofiber film, where rGO is reduced graphene oxide, by electrospinning, from which the MOF particles facing the S cathode were tightly adsorbed on the surfaces of PAN nanofibers and captured by chemical adsorption<sup>[17]</sup>. The rGO-PAN layer facing the Li anode side can maximize the uniform deposition of lithium ions to control the structural changes of the Li anode. The blocking effect alone, however, cannot prevent the consumption of the active substance, so adding a conductive component on the positive side will enable the conversion of the lithium polysulfide on the positive side, as well as reducing the interface resistance between the diaphragm and the positive electrode, and improving the utilization rate of the active material<sup>[18-23]</sup>. Therefore, it will be an effective strategy to design a functional separator with physical adsorption, chemical adsorption, and catalytic conversion, where polysulfides are adsorbed on the surface of the material by physical/chemical action and then catalytically reduced on the surface of the separator<sup>[24-28]</sup>. It is well known that gelatin has high ionic conductivity and a high ion migration number, so it can trap lithium polysulfide

while stabilizing lithium metal<sup>[29,30]</sup>.  $C_{60}$  provides the conversion sites for lithium polysulfide, and zeolitic imidazolate framework-67 (ZIF-67) provides the chemical adsorption sites<sup>[31,32]</sup>. The nanofiber membrane plays an important role in adsorption, conversion of polysulfides, and inhibition of lithium dendrite growth, improving the performance of lithium-sulfur batteries.

Therefore, in this work, a gelatin-based multifunctional composite separator (CZGNF) was designed and prepared by the electrospinning method. The CZGNF separator is a two-layer nanofibrous membrane with multiple functions. Gelatin with good ionic conductivity and high lithium-ion mobility is an excellent material for a separator. Gelatin can also achieve homogenization of the lithium-ion flux and improve the stability of lithium metal. In the CZGNF separator, polysulfides are chemisorbed by ZIF-67, preventing the shuttling of lithium polysulfides.  $C_{60}$  provides lithium polysulfide conversion sites and improves the conversion efficiency of Li polysulfides. The preparation of the CZGNF separator is simple, and it can effectively prevent the “shuttle effect” while improving the stability of the lithium anode. The performance of Li-S batteries is significantly improved. This article provides new ideas for the study of multifunctional composite nanofiber separators.

## EXPERIMENTAL METHODS

### Materials

Multi-walled carbon nanotubes (L-MWNT-1020 Shenzhen Nano Port), sublimed sulfur (AR, Aladdin),  $Co(NO_3)_2 \cdot 6H_2O$  (AR, Shanghai Hushi), 2-methylimidazole (99%, Aladdin), poly(vinylidene fluoride-co-hexafluoropropylene) (PVDF-HFP, molecular weight, MW = 400000), 1-methyl-2-pyrrolidinone (NMP, anhydrous, 99.5%, Aladdin), gelatin (Aladdin, Chemical purity (CP), Shanghai Aladdin Biochemical Technology Co., LTD), acetic acid (Sinopharm Chemical Reagent Co., Ltd.), methyl alcohol (99.8% from ACP Chemical Inc.),  $C_{60}$  (99.9%, Aladdin). All chemicals were purchased and used directly without further treatment.

### Preparation of ZIF-67

40 mmol 2-methylimidazole and 10 mmol  $Co(NO_3)_2 \cdot 6H_2O$  were separately dissolved in 100 mL of methanol and magnetically stirred for 0.5 h. Then, the 2-methylimidazole solution was slowly added to the  $Co(NO_3)_2 \cdot 6H_2O$  solution and magnetically stirred for 6 h. The resulting solution was left at room temperature for 24 h, and then washed with methanol and centrifuged 3 times. Finally, the precipitate was dried at 60 °C for 12 h to obtain purple ZIF-67 particles.

### Preparation of gelatin nanofiber and $C_{60}$ /ZIF-67-GNF separator

Preparation of the gelatin nanofiber (GNF) separator: 1.8 g of gelatin was added to 8 g acetic acid and 2 g distilled water and stirred for 12 h to obtain solution A. Electrospinning was performed with 10 mL of solution A at a high voltage of 16.5 kV at a rate of 0.09 mL h<sup>-1</sup>. The distance between the needle tip and the collector was set to 17 cm. The product was dried at 60 °C for 12 h and separated from Al foil to obtain the electrospun separator (GNF).

Preparation of the  $C_{60}$ /ZIF-67-GNF (CZGNF) separator: 0.1 g of ZIF-67, 0.1 g of  $C_{60}$ , and 1.8 g of gelatin were added to 8 g acetic acid and 2 g distilled water, followed by stirring for 12 h to obtain solution B. First, the electrospinning of solution A was conducted in a 4 mL injection pump. After that, the electrospinning of solution B was carried out in a 4 mL injection pump. Thus, fibrous separators of different compositions on both sides were obtained. Finally, the electrospun separator was treated in a drying oven at 60 °C for 12 h and separated from its Al foil to obtain the CZGNF composite separator. The electrospinning process parameters were the same as above.

### Preparation of positive electrode

Sublimated sulfur and multi-walled carbon nanotubes (MWCNTs) were ball-milled at a ratio of 4:1 for 12 h to obtain evenly mixed S/MWCNT materials. The S/MWCNT materials were kept in a reaction vessel at 155 °C for 12 h to obtain the S/MWCNT composite material. As shown in [Supplementary Figure 1](#), the sulfur ratio in S/MWCNT composite is 78.9%. The S/MWCNT composite material, Super P, and PVDF dissolved in NMP in a mass ratio of 7:2:1 to obtain the sulfur cathode slurry. Therefore, the content of sulfur in the cathode is  $78.9\% \times 70\% = 55.2\%$ . The obtained slurry was evenly coated on Al foil with a scraper and baked at 60 °C for 12 h. The mass loading of S in the electrode was about  $1.2 \text{ mg cm}^{-2}$ .

### Material characterization

The phase analysis of the material was performed with a D/MAX2500V rotating target X-ray diffractometer (XRD) at an angle of  $10^\circ$ - $40^\circ$ . Each material phase could then be determined by the position and intensity of the different characteristic peaks corresponding to the standard Powder Diffraction File (PDF). The surface morphology of the prepared materials was analyzed by using a Zeiss Gemini 500 thermal field emission scanning electron microscope. The corresponding X-ray energy dispersive spectrometer (EDS) was used for plane scanning to determine the type and distribution of elements. The morphology of the material was characterized by scanning electron microscopy (SEM). Gold spraying was carried out before SEM observations, and the spray time was set to 60 s.

### Battery assembly and measurements

The batteries were assembled with a CR2032 battery shell. The S/MWCNT composite material was used as the positive electrode and lithium metal as the negative electrode. Three different batteries were assembled with a polypropylene (PP) separator, a GNF separator, and a CZGNF separator, respectively. In the case of the CZGNF separator, the side containing ZIF-67 and  $C_{60}$  faced the positive electrode. The Li-S batteries employed 1.0 M lithium bis(fluoromethanesulfonyl)imide (LiTFSI) in dimethoxy ethane: dioxolane (DME: DOL, 1:1 v/v) with 2.0 %  $\text{LiNO}_3$  as the electrolyte additive. The electrolyte was 50  $\mu\text{L}$  and the electrolyte/sulfur ratio (E/S ratio) was  $27 \mu\text{L mg}^{-1}$  at the time of cell assembly. All the above operations were carried out in a glove box filled with Ar. Electrochemical tests of the assembled batteries were carried out, such as charging and discharge performance testing, cyclic performance testing, electrochemical impedance spectroscopy (EIS), cyclic voltammetry (CV), etc.

## RESULTS AND DISCUSSION

[Figure 1](#) shows the synthesis and functional structure of the CZGNF nanofiber separator. The separator is a two-layer structure, the first layer of pure gelatin-based nanofiber film is prepared by the electrospinning method, and then on the basis of this layer, the ZIF-67- $C_{60}$ -gelatin-based nanofiber separator is prepared by electrospinning method. Finally, the nanofiber separator is placed in an oven for drying to obtain the CZGNF separators with different functions on both sides. The CZGNF diaphragm facing the positive side can chemically adsorb polysulfides and provide conversion sites for lithium polysulfide, while the negative side can improve the amount of lithium-ion migration and prevent lithium dendrites from being generated.

In this work, gelatin was used as the separator substrate. Fourier transform infrared (FTIR) analysis of GNF separator was performed to verify its gelatin groups. [Figure 2A](#) shows that the characteristic peaks of gelatin groups are located around  $1200$ - $1650 \text{ cm}^{-1}$  and  $2900$ - $3100 \text{ cm}^{-1}$ <sup>[29]</sup>. Among them, the amine groups and carboxyl groups of gelatins are hydrophilic groups, so that gelatin has a good liquid absorption rate and the ionic conductivity of the gelatin substrate is improved. The XRD patterns of ZIF-67, GNF, and CZGNF [[Figure 2B](#)] reflect the phase structures of the three separators. The XRD pattern of CZGNF separator did not show strong reflections due to the low doping content of ZIF-67 particles, although the presence of cobalt element could be proved in EDS analysis. In addition, the main peak in the XRD pattern for the CZGNF separator corresponds to that of  $C_{60}$  (PDF#47-0787), which proves the successful doping of  $C_{60}$ .

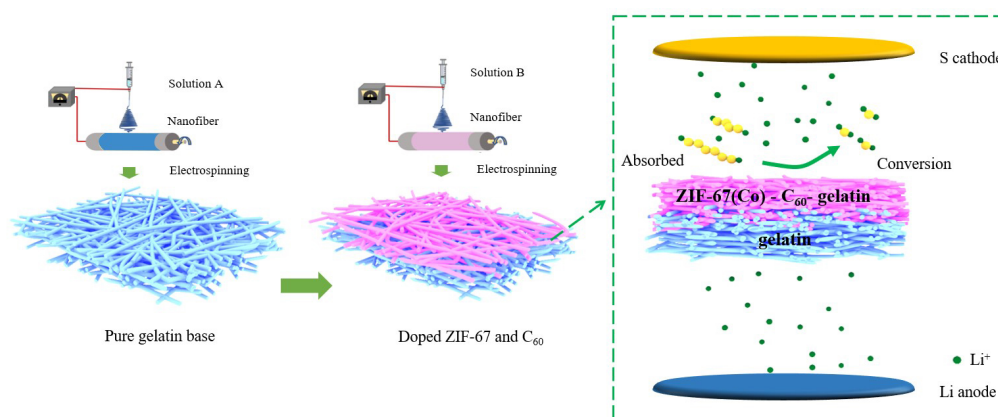


**Figure 1.** Schematic diagram of the synthesis and functional structure of the CZGNF separator.

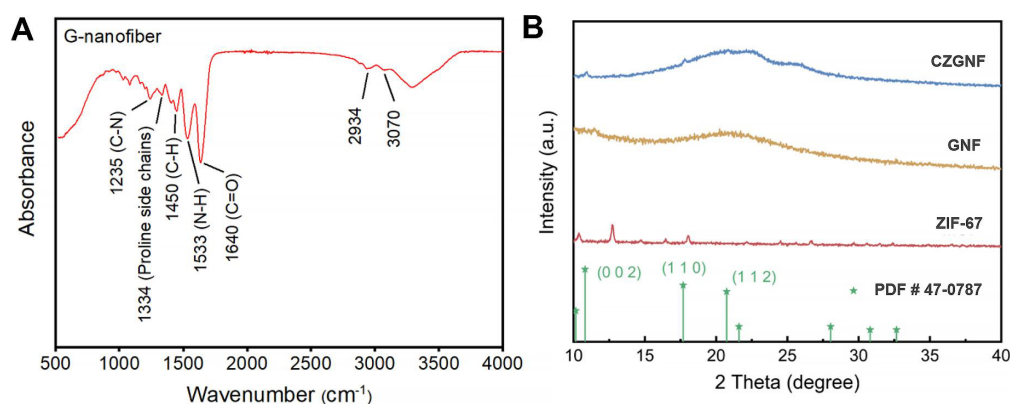


**Figure 2.** (A) FTIR spectrum of GNF; (B) XRD patterns of ZIF-67, GNF, and CZGNF.

Figure 3 displays the microstructure and fiber diameter distribution of the PP separator, GNF separator, and CZGNF separator. The surface of the PP separator presents irregular large pores with a width of about 600 nm-1  $\mu\text{m}$  [Figure 3A]. These large pores can pass not only lithium ions but also macromolecular lithium polysulfides, thus causing a serious “shuttle effect”. The GNF separator and CZGNF separator prepared by electrospinning exhibited the phenomenon of random intertwining of the, thus forming a three-dimensional (3D) fiber network structure [Figure 3B and C]. This fibrous mesh structure can effectively trap lithium polysulfide and prevent its diffusion to the lithium anode. After the addition of  $\text{C}_{60}$  and ZIF-67 particles, the separator facing cathode surface appeared light purple [Figure 3C]. The successful doping of  $\text{C}_{60}$  can be further proved by XRD pattern. In addition, there is no washing, pickling, etc. in the dissolution process. After the dissolution process, the solution is sprayed directly by electrospinning, so  $\text{C}_{60}$  and ZIF-67 were in the film certainly. Moreover, the color of ZIF-67 is purple, and the color of the prepared film facing the cathode is also light purple. Therefore, it can be determined that  $\text{C}_{60}$  and ZIF-67 have been successfully added. The CZGNF separator is white on one side and gray-purple on the other due to different spinning solutions. The thickness of the CZGNF separator is about 72  $\mu\text{m}$  [Figure 3D]. The main reason for the different morphology of GNF and CZGNF is the addition of  $\text{C}_{60}$  and ZIF-67, which leads to the increased electrical conductivity of the co-spun polymer nanofibers. Moreover, when the nanofibers are prepared by

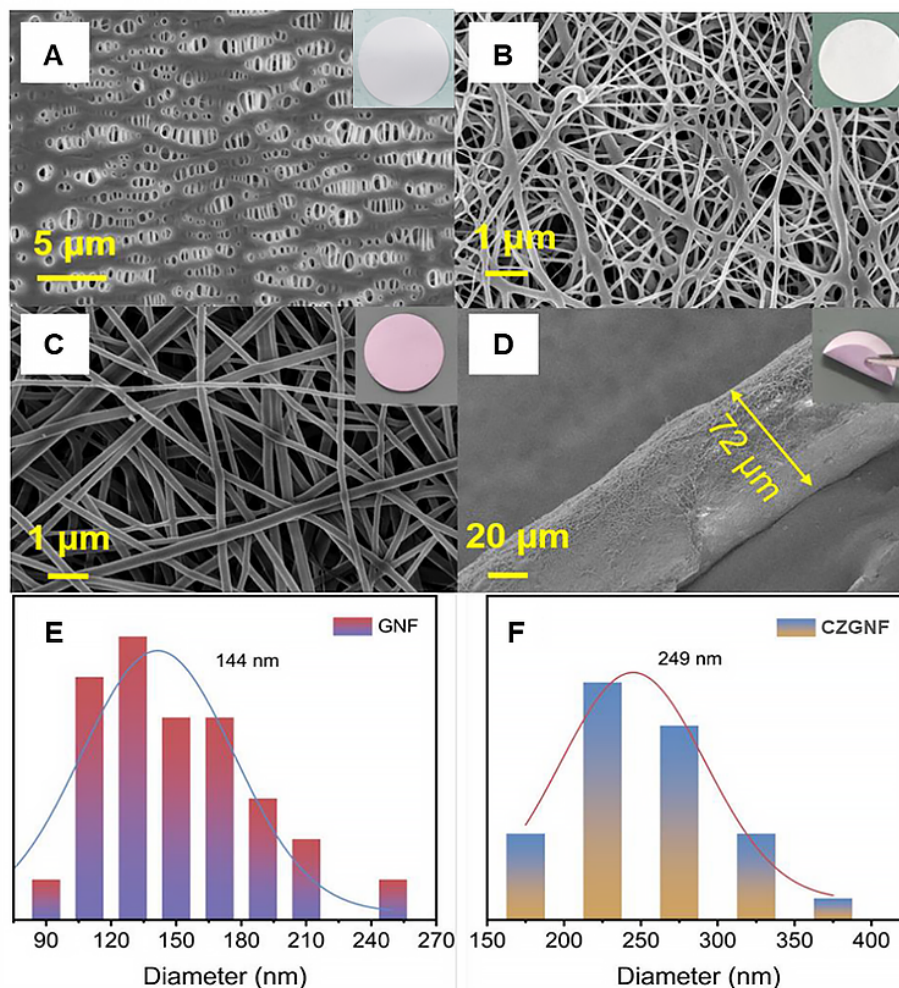


**Figure 3.** SEM images and photograph of the (A) PP separator; (B) GNF separator; and (C) the cathode side and (D) cross-section of CZGNF; diameter distributions of (E) GNF and (F) CZGNF.

electrospinning, the stretching effect of the electrostatic field on the solution will make the material exist mainly on the fiber surface and inside the fiber, which can significantly enhance the electrical conductivity and mechanical properties of the co-spun fiber film. There was no obvious delamination between the two separators after continuous electrospinning. Furthermore, the fibers on the cathode side of the CZGNF separator were rough, which proves the presence of functional particles on the cathode side. The fiber diameter of the GNF separator was 144 nm [Figure 3E]. The fiber diameter of CZGNF separator was 249 nm [Figure 3F]. The results indicated that  $C_{60}$  and ZIF-67 particles were successfully formed on the cathode side surface of the CZGNF separator. The CZGNF separator obtained by two consecutive electrospinnings avoids the method of adding two functional layers to the traditional separator to increase the ion transport resistance. Therefore, the CZGNF separator can effectively reduce the interfacial resistance. At the same time, the addition of  $C_{60}$  and ZIF-67 endows the two sides of the separator with different functions. Because the cathode side of the CZGNF separator converts lithium polysulfides by adsorption, the anode side enables uniform deposition of lithium ions.

Figure 4 shows SEM and EDS images of the cathode side and cross-section of CZGNF. We mainly studied the doping of Co element. The CZGNF separator presented a fibrous structure and an even distribution of

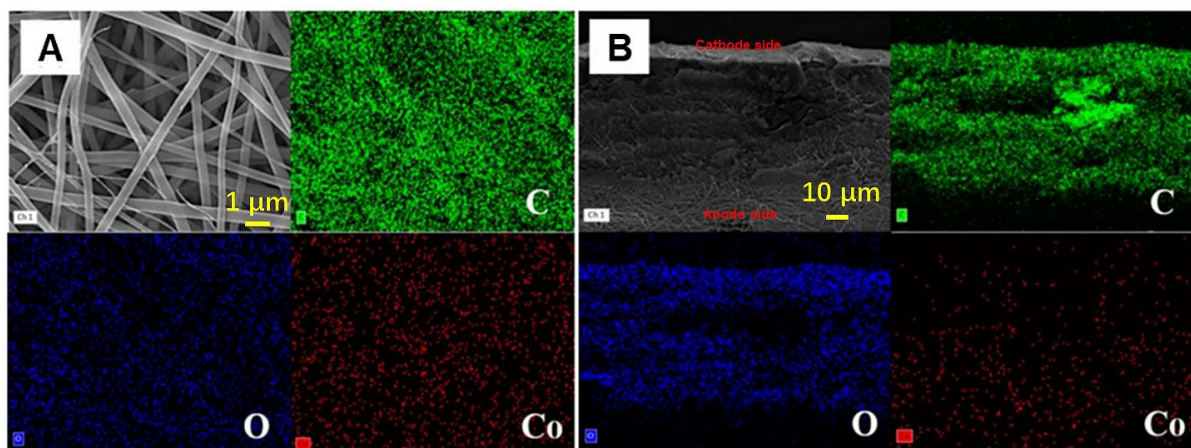


**Figure 4.** SEM images and corresponding EDS maps of (A) the side facing cathode and (B) a cross-section of the CZGNF separator.

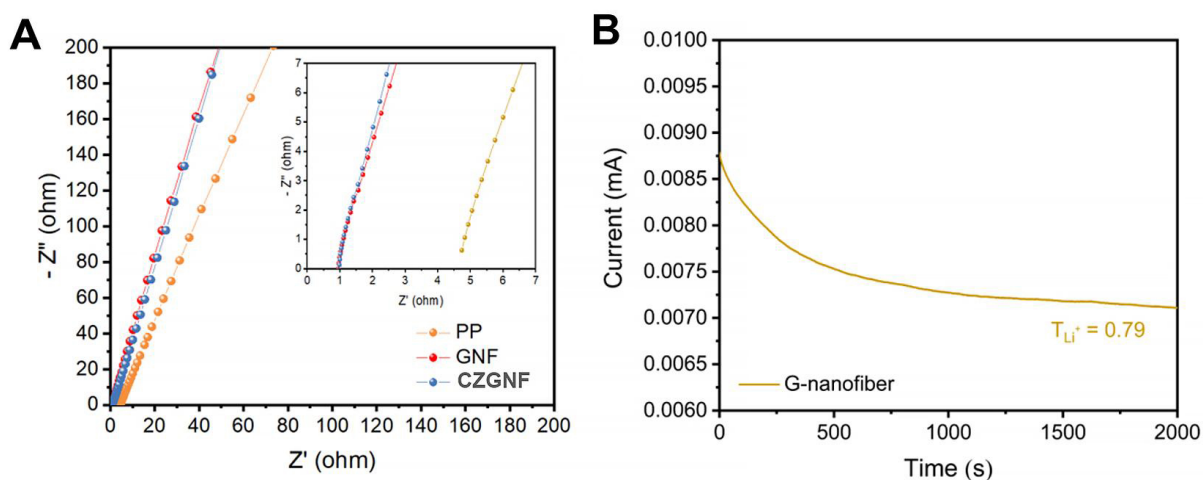


**Figure 5.** (A) Bulk impedance plots of PP separator, GNF separator, and CZGNF separator with enlargement in the inset; (B) lithium-ion transference number test of GNF separator.

Co element [Figure 4A], which proved the successful doping of ZIF-67 on the cathode side during electrospinning. The cross-section of the CZGNF separator exhibits a small amount of carbon accumulation in EDS analysis due to the change in the spinning solution during electrospinning [Figure 4B]. It can be seen from the EDS map that the Co element is mainly distributed in the fibers facing the cathode, indicating that the two sides of the CZGNF separator are composed of different components and have different functions. On the CZGNF separator, the lithium polysulfides are diffused to the positive electrode side, and the Co element chemically adsorbs the lithium polysulfides, so that the separator on the positive electrode side can effectively chemically adsorb the lithium polysulfides. The Co element chemisorbs lithium polysulfide in ZIF-67. The  $C_{60}$  can provide the transformation sites for lithium polysulfide. The lithium polysulfide adsorbed on ZIF-67 was rapidly converted, and the nucleation overpotential of lithium polysulfide was thereby reduced. The pure gelatin-based side of the CZGNF separator has good ionic conductivity and a high Li ion transfer number, which contributes to the uniformity of the Li flux.

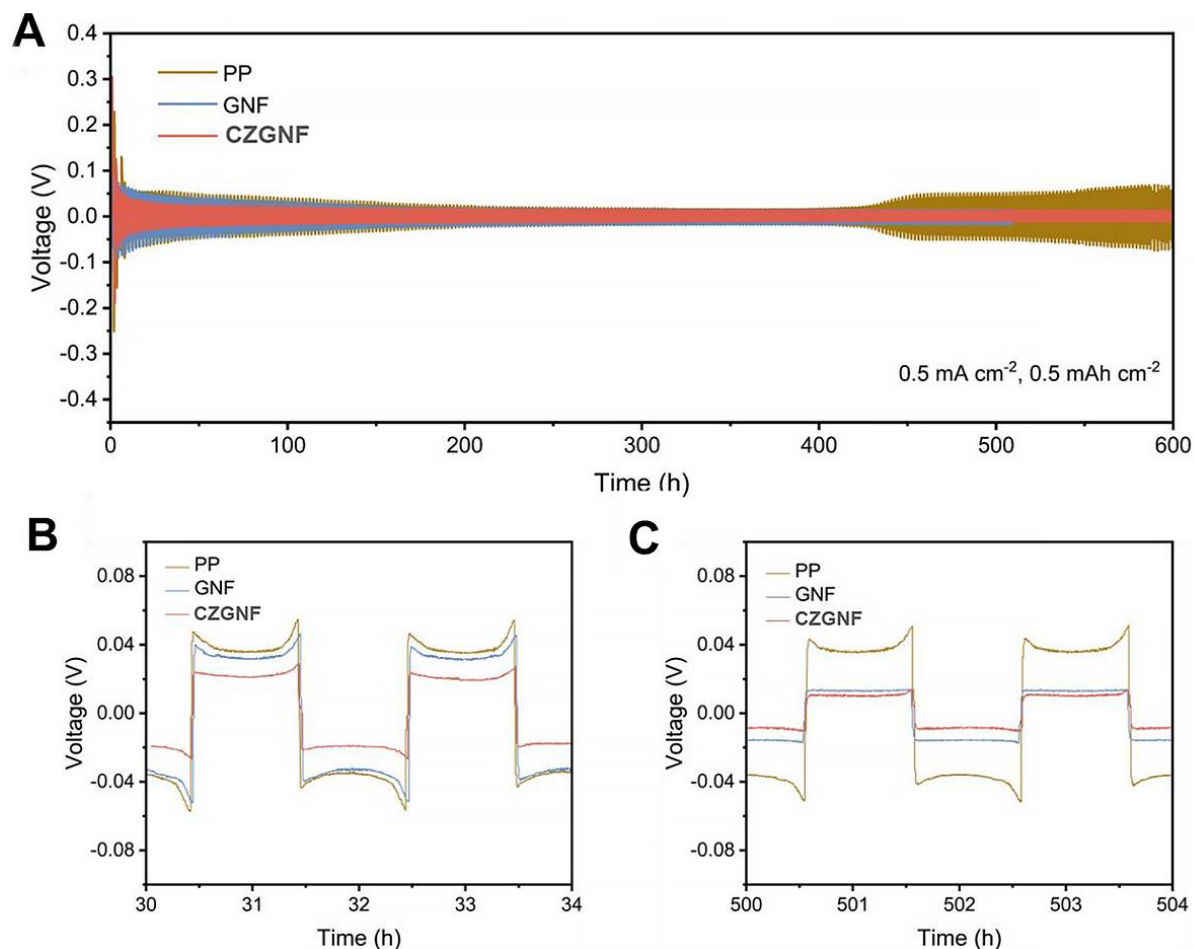


**Figure 6.** (A) The galvanostatic cycling performance of Li||Li symmetric batteries at  $0.5 \text{ mA cm}^{-2}$ ,  $0.5 \text{ mAh cm}^{-2}$ , and expanded views of (B) 30-34 h and (C) 500-504 h.

Figure 5 shows the bulk impedance curves of the three separators and the lithium-ion transfer number of the GNF separator. Ionic conductivity is an important parameter for separators. In order to test the separator body impedance ( $R$ ), the separator is sandwiched between stainless steel sheets (SS) and fully saturated with electrolyte to assemble the SS | separator | SS cell and perform the body impedance test. Separator ionic conductivity ( $\sigma$ ) can be calculated by the following equation [Equation 1]:

$$\sigma = \frac{A}{R \cdot S} \quad (1)$$

where  $A$  is separator thickness;  $R$  is bulk impedance;  $S$  is separator area. The bulk impedance of the PP separator is  $4.72 \Omega$ . The bulk impedance of both the GNF separator and the CZGNF separator is about  $1 \Omega$  [Figure 5A]. The ionic conductivity of PP separator, GNF separator, and CZGNF separator with the electrolyte of 1.0 M LiTFSI in DME: DOL (1:1 v/v) with 2.0 %  $\text{LiNO}_3$ , were  $2.63 \times 10^{-4} \text{ S cm}^{-1}$ ,  $3.08 \times 10^{-3} \text{ S cm}^{-1}$ , and  $3.58 \times 10^{-3} \text{ S cm}^{-1}$ , respectively. Therefore, the gelatin-based separator can greatly improve the ionic conductivity of the original PP separator and accelerate the electrochemical reaction speed of the battery.

The conductivity of the separator is composed of the migration rates of cations and anions. Relatively speaking, the migration rate of lithium ions is more important. Hence, it is necessary to increase the mobility of lithium ions while increasing the ionic conductivity of the separator. The characterization of lithium-ion migration number was achieved by applying a 10 mV initial voltage and dc polarization for measuring Li | separator | Li battery, and the separator was soaked with electrolyte before testing. The calculation for the lithium-ion migration number can be expressed as follows [Equation 2]:

$$T_{Li^+} = \frac{I_s}{I_o} \quad (2)$$

where  $I_s$  is the steady-state current,  $I_o$  is the initial current, and  $T_{Li^+}$  is the ion migration number. The  $T_{Li^+}$  of the GNF separator is higher than that of the PP separator. The  $T_{Li^+}$  of the GNF separator is 0.79 [Figure 5B]. The amino acids with negative charges were used as coordination sites for attracting anions (TFSI). The main chain oxygen in the gelatin polypeptide chain also has a strong affinity towards lithium ions. The result is that lithium ions can jump quickly between oxygen atoms. In consequence, the gelatin-based separator has higher lithium-ion transport efficiency than the ordinary PP separator, which can effectively avoid uniform lithium flux.

At the higher current density of  $0.5 \text{ mA cm}^{-2}$  and an areal capacity of  $0.5 \text{ mAh cm}^{-2}$ , the lithium ions cannot be deposited on the surface of the lithium metal thanks to the low ionic conductivity of the PP separator [Figure 6A]. The overpotential of the symmetric battery with PP separator increased rapidly after 400 h of cycling. In contrast, the symmetrical batteries with the GNF separator and CZGNF separator had good cycling stability. The polarization of symmetric batteries with CZGNF separator is lower than that of symmetric batteries with PP separator for cycling beyond 400 h. The polarization voltage of symmetrical batteries with PP separator and GNF separator is about 85 mV with cycling for 30-34 h. The polarization voltage of the symmetric battery with PP separator and GNF separator is larger than that of the symmetric battery with CZGNF separator [Figure 6B]. The reason is that the pore size of the GNF separator is too large and not fully activated in the previous cycles. As the cycling progresses, however, the overpotential of the symmetrical battery with GNF separator gradually decreases and tends to be stable. The polarization voltage of symmetric batteries with GNF or CZGNF separators is about 29 mV over 500-504 h of cycling [Figure 6C]. The polarization voltage of the symmetric batteries with the GNF separator and the CZGNF separator is lower than that of the symmetric battery with PP separator. The impedance plots of Li||Li symmetric batteries with PP, GNF and CZGNF separators after cycling for 100 h are also provided in Supplementary Figure 2. In conclusion, gelatin rapidly and steadily deposits lithium ions during the battery cycle and contributes to lithium nucleation.

Figure 7 displays the electrochemical performances of batteries assembled with different separators. The Li-S batteries with CZGNF separator have the highest initial discharge specific capacity of  $1358 \text{ mAh g}^{-1}$ . The initial discharge capacity of Li-S battery with GNF separator is  $1334 \text{ mAh g}^{-1}$ . The initial discharge capacity of Li-S battery with PP separator is the lowest [Figure 7A]. In short, the Li-S batteries with CZGNF separator had the highest utilization rate of sulfur active materials. The utilization rate of sulfur active material was 81.1%. Therefore, the use of gelatin as the separator substrate can effectively reduce the loss of sulfur in the active material. The conversion of soluble lithium polysulfide lithium was promoted by  $C_{60}$  and ZIF-67 to form insoluble  $Li_2S_2/Li_2S$ . Figure 7B shows the second plateau of the discharge curves of Li-S batteries with three separators. The overpotential was 20 mV for the GNF separator, 18 mV for the PP

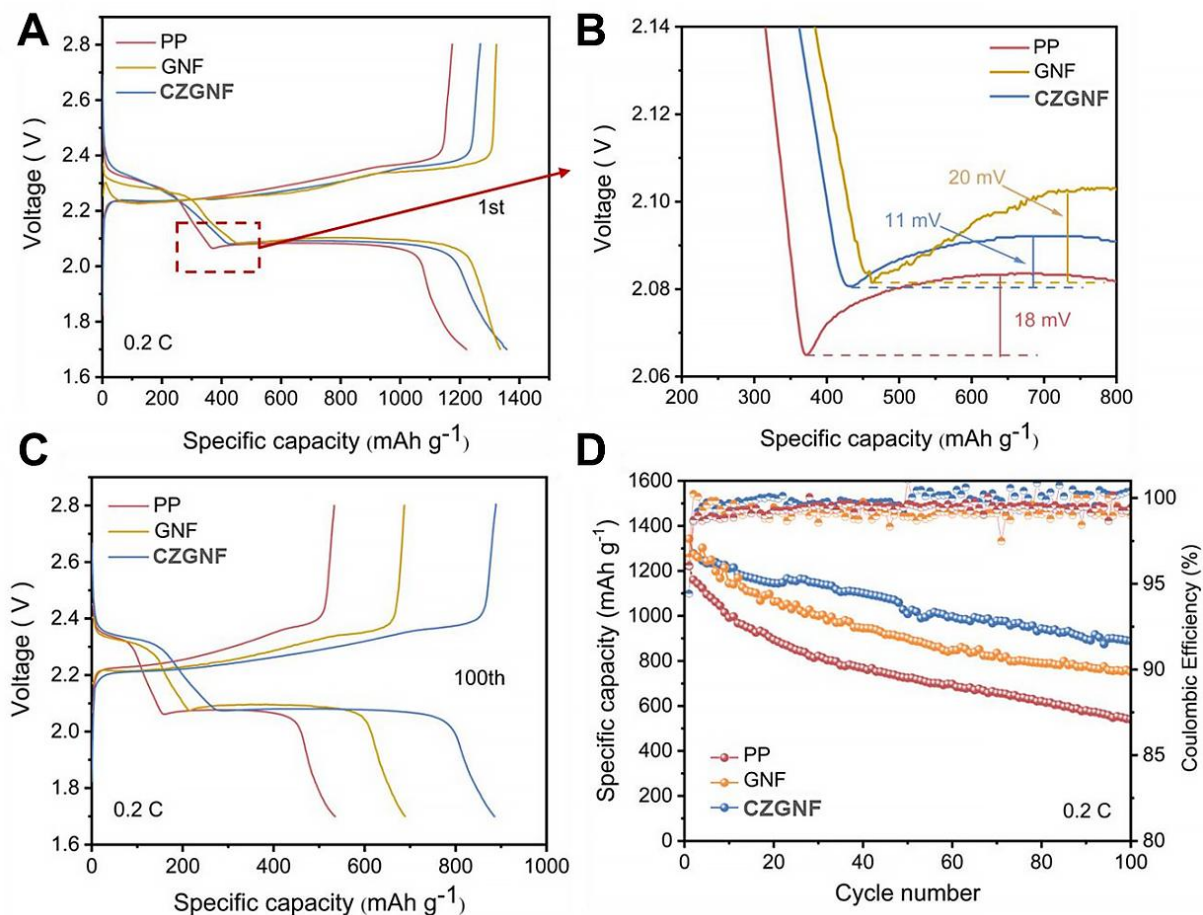


**Figure 7.** (A) The 1st cycle charge-discharge curves; (B) magnified discharge curves; (C) 100<sup>th</sup> cycle charge-discharge curves; and (D) cycling performances of the Li-S batteries with different separators at 0.2 C.

separator, and 11 mV for the CZGNF separator, so the Li-S battery with CZGNF separator had the smallest overpotential. Thus, the CZGNF separator improved the liquid-solid conversion kinetics of lithium polysulfide. Three quarters of the theoretical capacity of the sulfur cathodes came from the deposition of soluble lithium sulfide to be converted to insoluble  $\text{Li}_2\text{S}$ , so it is important for rapid polysulfide transition kinetics and abundant deposition sites, which facilitate the cycling performance of Li-S batteries [33]. For the Li-S battery with CZGNF separator after 100 cycles, the specific discharge capacity remained at  $888 \text{ mAh g}^{-1}$ , and the capacity retention rate was 65.4%. The discharge specific capacities of Li-S batteries with GNF and PP separators after 100 cycles were  $750 \text{ mAh g}^{-1}$  and  $539 \text{ mAh g}^{-1}$ , respectively, and their capacity retention rates were 56.2% and 44.1%, respectively [Figure 7C and D]. The presence of a slight shuttle effect may lead to unstable and excessive discharge/charge efficiency of lithium-sulfur batteries [34]. Therefore, the Coulombic efficiency of Li-S batteries with CZGNF separator is higher than those of Li-S batteries with GNF separator and PP separator. The Li-S battery with CZGNF separator had the highest initial capacity, the highest capacity retention rate, and the highest Coulombic efficiency due to fast ion/electron diffusion and high lithium polysulfide conversion efficiency.

Figure 8 shows the electrochemical impedance spectra (EIS) of the Li-S batteries with three separators before and after cycling. The Li-S battery with CZGNF separator has the lowest impedance value because of the high ionic conductivity of the CZGNF separator, which accelerates electron transfer inside the battery

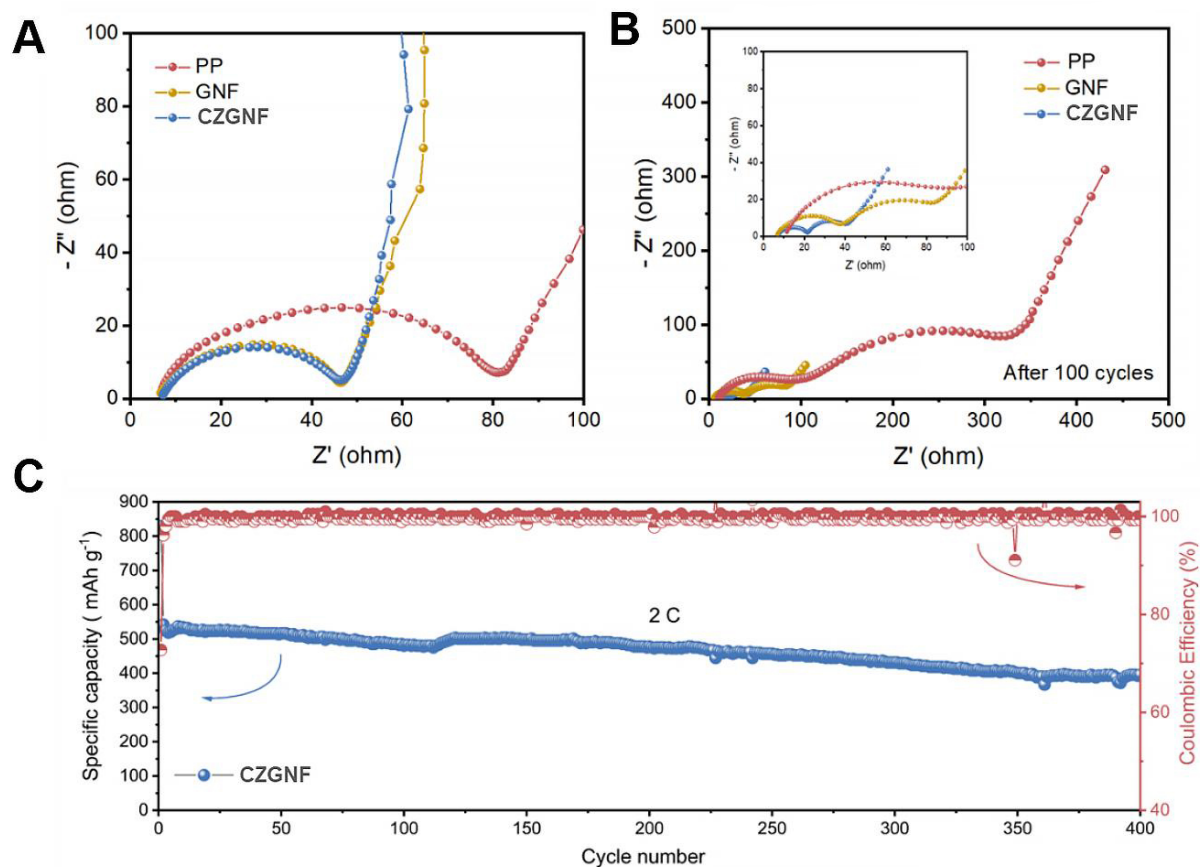


**Figure 8.** EIS spectra of Li-S batteries containing the different separators (A) before and (B) after cycling, with enlargement in the inset; (C) long cycle life tests of Li-S batteries based on CZGNF separator under 2 C.

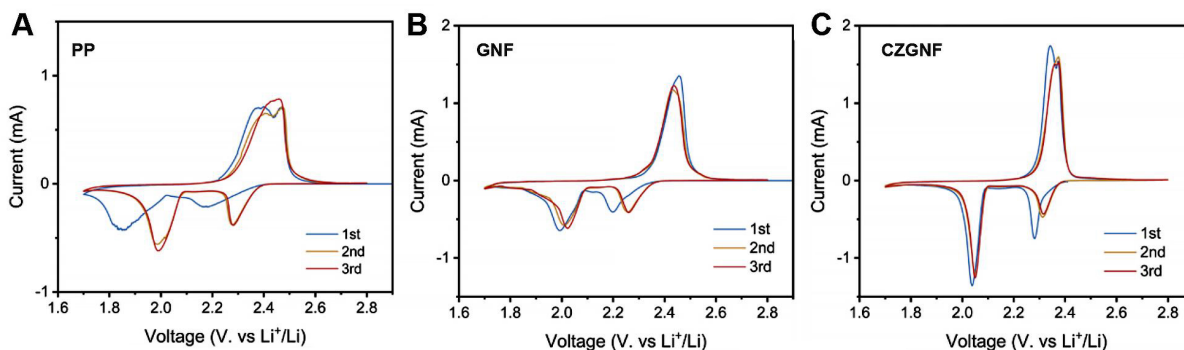


**Figure 9.** CV curves of Li-S batteries with different separators: (A) PP separator; (B) GNF separator; (C) CZGNF separator.

and accelerates the oxidation reaction kinetics [Figure 8A]. The battery impedance decreases slightly after cycling due to the gradual penetration of the electrolyte into the electrode and the re-diffusion of sulfur on the electrode surface [Figure 8B]. The Li-S battery with CZGNF separator yielded a capacity retention rate of 72.9% after 400 cycles at 2 C [Figure 8C]. The excellent performance of Li-S batteries with CZGNF separators is owing to the gelatin matrix of the separator with its high ion migration number and the fast transport of lithium ions, as well as the strong capture and catalysis of lithium polysulfides by ZIF-67 particles and C<sub>60</sub>, improving the redox kinetics of the bulk sulfur.

Figure 9 displays the cyclic voltammetry curves (CV) of Li-S batteries with the three different separators. All the batteries with the three kinds of separators showed two reduction peaks and one oxidation peak. The CZGNF separator provided the highest reduction peak and the lowest oxidation peak, which proved that the ZIF-67 particles and C<sub>60</sub> in the CZGNF separator accelerated the conversion of lithium polysulfides and reduced the difficulty of liquid/solid conversion of lithium sulfide batteries. The Li-S battery with CZGNF separator had the sharpest CV curve peak, which further proves its rapid redox reaction kinetics.

## CONCLUSION

In conclusion, a gelatin-based nanofiber separator doped with C<sub>60</sub> and ZIF-67 was constructed by electrostatic spinning of two different solutions. It can be used as a multifunctional separator for Li-S batteries. The CZGNF separator provides not only adsorption sites for lithium polysulfide, but also conversion sites for lithium polysulfide, leading to improved conversion efficiency. Gelatin was used as the separator substrate, not merely because it has very high ionic conductivity, but also because it has a high lithium-ion transfer number, which improved the stability of the symmetric battery and kept the lithium metal stable. The Li-S batteries with CZGNF separator were more stable than Li-S batteries with PP separator. Li||Li symmetric batteries with CZGNF separator remained stable for more than 600 h at 0.5 mA cm<sup>-2</sup>. In particular, after 100 cycles at a current density of 0.2 C, the discharge specific capacity of an Li-S battery with CZGNF separator was maintained at 888 mAh g<sup>-1</sup>, and the capacity retention rate of Li-S batteries was 72.9% after 400 cycles at 2 C, which means that there is good capacity retention rate and that the batteries have better application prospects in future battery development.

## DECLARATIONS

### Authors' contribution

Designed the research and funding acquisition: Liang X

Writing - draft: Liang X

Writing - original draft: Zhao D

Data collection and experiment: Wang L

Data collection and analysis: Zhao D, Huang Q

Data analysis: Deng C, Wang L, Liang S, Hu L

Review and editing: Liang X, Deng C, Wang L

Refining the ideas and finalizing this paper: Deng H, Xiang H

### Availability of data and materials

Not applicable.

### Financial support and sponsorship

Financial support provided by the National Natural Science Foundation of China (Grant Nos. 21606065, 52072105, 21676067, 51972093, and 51902079), Anhui Provincial Natural Science Foundation (Grant Nos. 2208085ME108, 1708085QE98, 1908085QE178, and 2008085QE271), the Fundamental Research Funds for the Central Universities (Grant Nos. PA2021KCPY0028, PA2021GDGP0059, JZ2018HGBZ0138, JZ2020YYPY0109, and PA2020GDJQ0026), the Key Technologies Research and Development Program of Anhui Province (Grant No. 202104a05020044, 201904b11020040), the Major Science and Technology Projects in Anhui Province (Grant Nos. 2021e03020001 and 202003a05020014), the Key Projects for the Excellent Talent Foundation of Education Department of Anhui Province (No. gxyqZD2021136), the Top Discipline Talents Foundation of Anhui Province Educational Committee (gxbjZD2021085), and the University Natural Science Research Project of Anhui Province (KJ2021A1016) are gratefully acknowledged. Many thanks also go to Dr. Tania Silver for critical reading of the manuscript and valuable remarks.

### Conflicts of interest

All authors declared that there are no conflicts of interest.

### Ethical approval and consent to participate

Not applicable.

### Consent for publication

Not applicable.

### Copyright

© The Author(s) 2023.

## REFERENCES

1. Jiang L, Wang Z, Pan P, et al. Excimer ultraviolet-irradiated graphene separator for suppressing polysulfide shuttling in Li-S batteries. *J Alloys Compd* 2022;903:163932. DOI
2. Zhang L, Chen Y. Electrolyte solvation structure as a stabilization mechanism for electrodes. *Energy Mater* 2022;1:100004. DOI
3. Yu Z, Shao Y, Ma L, et al. Revealing the sulfur redox paths in a Li-S battery by an In situ hyphenated technique of electrochemistry and mass spectrometry. *Adv Mater* 2022;34:e2106618. DOI PubMed
4. Huang CJ, Thirumalraj B, Tao HC, et al. Decoupling the origins of irreversible coulombic efficiency in anode-free lithium metal batteries. *Nat Commun* 2021;12:1452. DOI PubMed PMC
5. Zheng S, Zhu X, Ouyang Y, et al. Metal-organic framework decorated polymer nanofiber composite separator for physiochemically shielding polysulfides in stable lithium-sulfur batteries. *Energy Fuels* 2021;35:19154-63. DOI
6. Chadha U, Bhardwaj P, Padmanaban S, et al. Review - contemporary progresses in carbon-based electrode material in Li-S batteries. *J Electrochem Soc* 2022;169:020530. DOI
7. Suzanowicz AM, Lee Y, Lin H, Marques OJJ, Segre CU, Mandal BK. A new graphitic nitride and reduced graphene oxide-based sulfur cathode for high-capacity lithium-sulfur cells. *Energies* 2022;15:702. DOI
8. Zhong X, Wang D, Sheng J, et al. Freestanding and sandwich mxene-based cathode with suppressed lithium polysulfides shuttle for flexible lithium-sulfur batteries. *Nano Lett* 2022;22:1207-16. DOI PubMed
9. Wei Z, Wang R. Chemically etched CeO<sub>2-x</sub> nanorods with abundant surface defects as effective cathode additive for trapping lithium polysulfides in Li-S batteries. *J Colloid Interf Sci* 2022;615:527-42. DOI
10. Chen X, Ji H, Chen W, et al. In situ protection of a sulfur cathode and a lithium anode via adopting a fluorinated electrolyte for stable lithium-sulfur batteries. *Sci China Mater* 2021;64:2127-38. DOI
11. Wang Q, Wang H, Wu J, Zhou M, Liu W, Zhou H. Advanced electrolyte design for stable lithium metal anode: from liquid to solid. *Nano Energy* 2021;80:105516. DOI
12. Paul PP, Mcshane EJ, Colclasure AM, et al. A review of existing and emerging methods for lithium detection and characterization in Li-ion and Li-metal batteries. *Adv Energy Mater* 2021;11:2100372. DOI
13. Balaish M, Gonzalez-rosillo JC, Kim KJ, Zhu Y, Hood ZD, Rupp JLM. Processing thin but robust electrolytes for solid-state batteries. *Nat Energy* 2021;6:227-39. DOI
14. Hu W, Liang X, Yang X, et al. Sulfophenylated poly (ether ether ketone ketone) nanofiber composite separator with excellent electrochemical performance and dimensional thermal stability for lithium-ion battery via electrospinning. *Macromol Mater Eng* 2021;306:2100118. DOI
15. Aslam MK, Jamil S, Hussain S, Xu M. Effects of catalysis and separator functionalization on high energy lithium sulfur batteries: a complete review. *Energy Environ Mater* 2022;Online ahead of print. DOI
16. Xiang H, Liu X, Deng N, Cheng B, Kang W. A novel EDOT/F co-doped PMIA nanofiber membrane as separator for high-performance lithium-sulfur battery. *Chem Asian J* 2022;17:e202200669. DOI PubMed
17. Zhou C, He Q, Li Z, et al. A robust electrospun separator modified with in situ grown metal-organic frameworks for lithium-sulfur batteries. *Chem Eng J* 2020;395:124979. DOI
18. Zhao J, Yan G, Zhang X, et al. In situ interfacial polymerization of lithiophilic COF@PP and POP@PP separators with lower shuttle effect and higher ion transport for high-performance Li-S batteries. *Chem Eng J* 2022;442:136352. DOI
19. Liang X, Wang L, Wang Y, Liu Y, Sun Y, Xiang H. Constructing multi-functional composite separator of PVDF-HFP/h-BN supported Co-CNF membrane for lithium-sulfur batteries. *Sustain Energy Fuels* 2022;6:440-8. DOI
20. Zhu L, Jiang H, Ran W, et al. Turning biomass waste to a valuable nitrogen and boron dual-doped carbon aerogel for high performance lithium-sulfur batteries. *Appl Surf Sci* 2019;489:154-64. DOI
21. Jing W, Zu J, Zou K, et al. Sandwich-like strontium fluoride graphene-modified separator inhibits polysulfide shuttling and lithium dendrite growth in lithium-sulfur batteries. *J Mater Chem A* 2022;10:4833-44. DOI
22. Han Y, Xu Y, Zhang S, Li T, Ramakrishna S, Liu Y. Progress of improving mechanical strength of electrospun nanofibrous

- membranes. *Macromol Mater Eng* 2020;305:2000230. DOI
23. Jiang W, Han Y, Ding Y. Sepiolite and ZIF-67 co-modified PAN/PVdF-HFP nanofiber separators for advanced Li-ion batteries. *Nanotechnology* 2022;33:425601. DOI PubMed
  24. Li B, Pan Y, Luo B, et al. MOF-derived NiCo<sub>2</sub>S<sub>4</sub>@C as a separator modification material for high-performance lithium-sulfur batteries. *Electrochim Acta* 2020;344:135811. DOI
  25. Huang S, Huixiang E, Yang Y, Zhang Y, Ye M, Li CC. Transition metal phosphides: new generation cathode host/separator modifier for Li-S batteries. *J Mater Chem A* 2021;9:7458-80. DOI
  26. Wang Y, Zhu L, Wang J, Zhang Z, Yu J, Yang Z. Enhanced chemisorption and catalytic conversion of polysulfides via CoFe@NC nanocubes modified separator for superior Li-S batteries. *Chem Eng J* 2022;433:133792. DOI
  27. Wei Z, Ren Y, Sokolowski J, Zhu X, Wu G. Mechanistic understanding of the role separators playing in advanced lithium-sulfur batteries. *InfoMat* 2020;2:483-508. DOI
  28. Li C, Liu R, Xiao Y, Cao F, Zhang H. Recent progress of separators in lithium-sulfur batteries. *Energy Stor Mater* 2021;40:439-60. DOI
  29. Chen M, Chen Z, Fu X, Zhong W. A Janus protein-based nanofabric for trapping polysulfides and stabilizing lithium metal in lithium-sulfur batteries. *J Mater Chem A* 2020;8:7377-89. DOI
  30. Chen M, Fu X, Taylor ND, Chen Z, Zhong W. Rational design of graphite nanoplatelets interlayers via a surfactant-controlled strategy for enhancing lithium-sulfur batteries. *ACS Sustain Chem Eng* 2019;7:15267-77. DOI
  31. Wu J, Wang S, Lei Z, et al. Pomegranate-like C<sub>60</sub>@cobalt/nitrogen-codoped porous carbon for high-performance oxygen reduction reaction and lithium-sulfur battery. *Nano Res* 2021;14:2596-605. DOI
  32. Zhao W, Feng W, Chen J, Niu Y, Zhang L. Polar Co<sub>3</sub>Se<sub>4</sub> nitrogen-doped porous carbon derived from ZIF-67 for use as a sulfur substrates in high-performance lithium-sulfur batteries. *J Alloys Compd* 2022;923:166435. DOI
  33. Li Y, Zhou P, Li H, et al. A freestanding flexible single-atom cobalt-based multifunctional interlayer toward reversible and durable lithium-sulfur batteries. *Small Methods* 2020;4:1900701. DOI
  34. Xu W, Pang H, Zhou H, et al. Lychee-like TiO<sub>2</sub>@TiN dual-function composite material for lithium-sulfur batteries. *RSC Adv* 2020;10:2670-6. DOI